Wetting transition of sessile and condensate droplets on copper-based superhydrophobic surfaces

Yugang Zhao[1], Hui Zhang[1], Wei Wang[2], Chun Yang[1]*

1 School of Mechanical and Aerospace Engineering, Nanyang Technological University, 50 Nanyang Avenue, Singapore 639798

2 Singapore Institute of Manufacturing Technology, 2 Fusionopolis Way, Singapore 138634

*E-mail: mcyang@ntu.edu.sg; Tel: (+65) 6790-4883

ABSTRACT:

Superhydrophobic state on natural materials and synthesized surfaces has been exploited in a broad range of technologies including thermal management, water harvesting, anti-icing, and flow control. However, under certain circumstances wetting transition from Cassie's mode to Wenzel's mode becomes inevitable. Such wetting transition degrades the performance of superhydrophobic surfaces and limits their applicability. Here, we report distinct wetting stabilities of two copper-based superhydrophobic surfaces which are with nano-asperities (diameter ~ 70 nm) of different packing density. Both the static (sessile droplet) and dynamic (dropwise condensation) wetting stabilities of the two surfaces are characterized. We show both theoretically and experimentally that sessile droplets on the surfaces of densely packed nano-asperities (pitch ~ 120 nm) can remain in stable Cassie's mode, while the wetting transition from Cassie's mode to Wenzel's mode occurs spontaneously on the surfaces of coarsely packed nano-asperities (pitch ~ 300 nm). The apparent contact angle on the surfaces of coarsely packed nano-asperities reduces from over 150^o to around 110^o, and the sliding angle increases from less than 5^o to over 60 ^{o} within 200 s, whereas the changes of both angles on the surfaces of densely packed nano-asperities are not noticeable. We also find that in dropwise condensation,

condensed droplets on the surfaces of densely packed nano-asperities maintain a stable Cassie's mode, while condensate droplets on the surfaces of coarsely packed nano-asperities are in Wenzel's mode. Exploiting the coupling effects of surface topography and wetting behaviors can open up existing vistas on surface engineering, leading to durable and sustainable surface design for diverse applications such as dropwise condensation and boiling heat transfer.

KEYWORDS: *wetting transition, superhydrophobicity, nanostructure, dropwise condensation*

1. Introduction

The purposeful design of generating micro/nano scale asperities and modulating interfacial energy to achieve surfaces with specific wetting properties is of great importance due to the significance from both fundamental and application viewpoints [1-8]. Roughness-induced superhydrophobicity, usually referred to as "the lotus leaf effect", is one of the well-known surface designs from this aspect. The study of superhydrophobicity has gained intensive attention recently, due to the outstanding performances of superhydrophobic surfaces in diverse applications, such as condensation/frosting heat transfer [9-14], self-cleaning [15-17], antifouling coating [18, 19], and drag reduction and flow control in smart microfluidic and lab-on-chip devices [20-23]. Despite most of superhydrophobic surfaces are characterized by using apparent contact angle larger than 150^{o} and small sliding angle, their wetting mode and stability can vary largely. The degradation of hydrophobicity also becomes inevitable as a result of liquid imbibition and boundary pinning effect [24-27], particularly in the cases of condensation [28-30] and droplet impact [31]. The underlying physics associated with wetting stability remains incomplete [32-35], which makes it challenging to achieve optimal design and process control of the performance of superhydrophobic surfaces.

When placing a water droplet onto a rough superhydrophobic surface, wetting occurs in accordance with a composite state (Cassie's mode) with many micrometer/nanometer sized air pockets trapped underneath the droplet, yielding a partially wetted surface. The contact interface is thus comprised of air/water and water/solid interfacial components. An irreversible transition from the metastable Cassie's mode to the stable Wenzel's mode can be triggered by external stimuli such as Laplace pressure, kinetic impact, thermal perturbation and phase changes. The ability of a rough superhydrophobic solid surface to resist this wetting transition depends on geometry and packing density of the asperities. Identifying a universal criterion for wetting in a stable Cassie's mode is thus the key to developing novel functionalized surfaces.

In this work, we study the wetting stability of two types of superhydrophobic copper surfaces packed with nano-asperities (~ 70 nm in diameter), to explore the effect of the packing density of asperities on the surface wetting behavior. We fabricated these two types of the copper surfaces using the electrochemical deposition method via simply changing the deposition rate such that the smaller deposition rate produced a relatively large packing density (~ 120 nm in pitch), and the larger deposition rate produced a relatively small packing density (~ 300 nm in pitch). We characterized the wetting stability of these surfaces in two cases: a) the evolution of static contact angle and sliding angle for a sessile water droplet; b) the dynamic wetting behavior during dropwise condensation. We found that the wetting on the surface with densely packed nano-asperities shows a stable Cassie's mode, and the wetting transits to Wenzel's mode spontaneously on the surface with coarsely packed nano-asperities. The different dynamic wetting behaviors also lead to different regimes of inter-drop coalescence during the dropwise condensation. The findings of the present study can shed light on the design of durable and

sustainable superhydrophobic surfaces which have wide applications such as condensation and boiling heat transfer.

2. Experimental section

2.1 Preparation of sample surfaces

As copper is a typical structural material used in heat exchangers, we chose thin copper plates as substrates, and fabricated two types of copper surfaces in this study. We used commercially available copper plates of 99.9% purity, and with a thickness of D = 1 mm and a square cut of 2 × 2 cm^2. The sample substrates were first polished using P800, P2000 and P6000 sand papers (with grit sizes of 21.8 μm, 10.3 μm and 4.0 μm, respectively) subsequently and followed by ultrasonication for 30 mins to remove any residues from polishing. After that, the sample substrates were immersed in 1 M hydrochloride acid solution and then placed in another ultrasonic bath for 20 mins to remove the oxidized film. Then, each substrate was cleaned using a standard protocol comprising of rinsed with acetone, ethanol, isopropyl alcohol, and deionized water subsequently and finally dried with nitrogen gas flow.

Nano-asperities were created on the aforementioned, pre-treated copper substrates using an electrochemical deposition method. The electrochemical deposition experiments were performed in a customized electrochemical reaction chamber, consisting of two copper electrodes (Anode as the source, and Cathode as the target substrate) and a chemical reagent, driven by a DC power supply. The chemical reagent used as the electrolyte solution was $CuCl_2$ with a fixed concentration of 100 mM. Two types of surfaces were prepared using different deposition rates. Surf_1 was generated with an electrical current density of 0.02 A/cm^2 and a coating time of 100 s; while Surf_2 was generated with an electrical current density of 0.1 A/cm^2 and a coating time of

20 s. Setting $m = \frac{ItM}{2eN_A}$ as the deposited mass per unit area (where I is the current density, t is the deposition time, M is the molecule weight of Cu, e is the elementary charge and N_A is the Avogadro constant), the deposition density of the two types of surfaces was the same with its magnitude as 670 ± 7.4 μg/cm^2.

To promote hydrophobicity, a self-assembled monolayer of fluorinated silane (trichloro (1H, 1H, 2H, 2H-perfluorooctyl) (Sigma-Aldrich) was deposited onto the copper substrates with nano-asperities via chemical vapor deposition (P < 0.01MPa). This self-assembled monolayer layer has a typical static contact angle of around 108.2 ± 0.5^o when applied to a smooth surface (as seen in the supporting information Figure S1). Prior to each experiment, the substrates were rinsed with DI water again for 2 mins to remove dust and other contaminants.

2.2 Surface characterizations

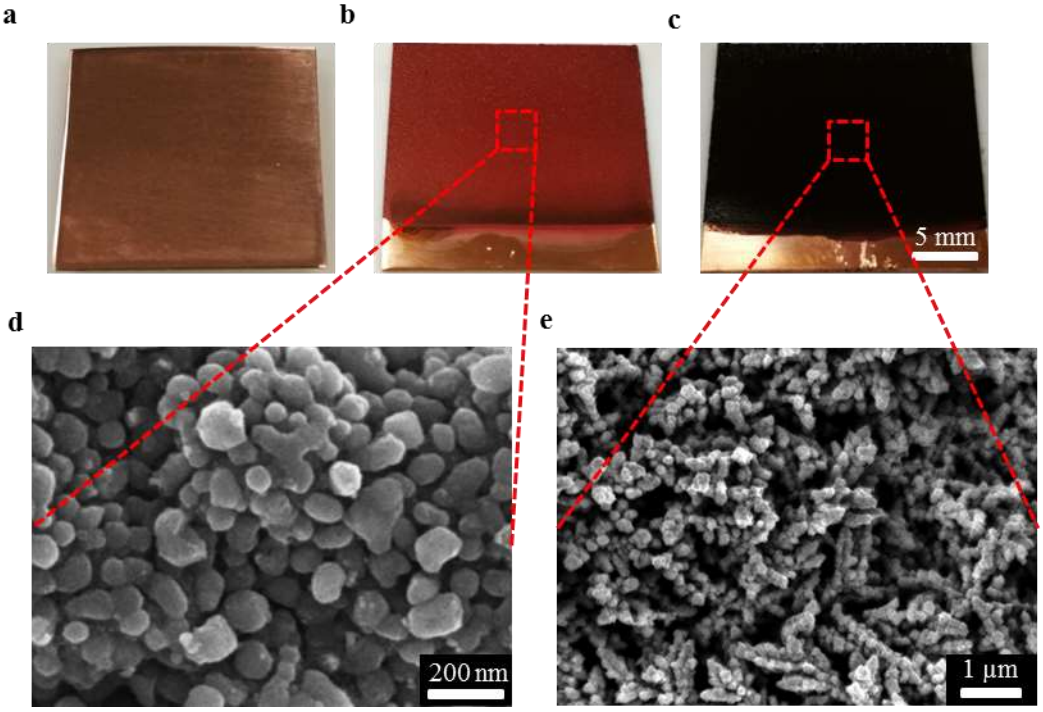

Figure 1. The physical appearance and nanoscale topography of the prepared surfaces: (a), (b) and (c) are photographs of an untreated copper surface, a surface produced from a small deposition rate, and a surface produced from a large deposition rate, respectively. (d) and (e) respectively show topography of nano-asperities for (b) and (c) by using a field emission scanning electronic microscope.

Electrochemically deposited copper has been used in numerous applications that require a wide range of mechanical and physical properties. In most situations, however, atomically smooth glassy coating with shining appearance is preferred [36]. In the present study, we deployed an unusual large deposition rate to obtain coarse nucleation sites and a large growth rate of copper clusters, providing the essential roughness for achieving superhydrophobicity [37, 38].

Figures 1(a), 1(b) and 1(c) show photographs of a bare copper substrate and two prepared substrates; the latter were obtained from the electrochemical deposition and the silanization. The prepared copper substrate from a small deposition rate (Surf_1) appears a bright red color. The substrate from a large deposition rate (Surf_2), however, shows completely different appearance of a dark black color. As these substrates are all made of the same material (pure copper), this difference in appearance is attributed to the absorption wavelength shift due to different surface nanostructures [39, 40].

Figures 1(d) and 1(e) show the topography of nano-asperities for the two fabricated substrates using a field emission scanning electronic microscope (FESEM, JEOL7600). For Surf_1 fabricated with a small deposition rate, spherical / semi-spherical copper crystals with an aspect ratio close to unity one are densely packed on the substrate. For Surf_2 fabricated with a large deposition rate, however, copper crystals form pointy clusters with a large aspect ratio and are coarsely packed on the substrate.

The topography of nano-asperities is resulted from the growth of copper nanocrystals during the deposition process. Recent studies reported that the growth of copper crystals varies for different combinations of electrical current density, electrolyte concentration and pH value [41]. As shown in the present study, changing the deposition rate is an effective approach to alter the copper crystalline structure and nano scale roughness. At a small deposition rate, copper crystals with scattered energetically preferential spheres/semi-spheres are seen. With enough time for the alignment of these crystals, they accumulate layer by layer and eventually form a planar interface with homogeneous distributions of copper crystals. At a large deposition rate, however, facet copper crystals form tall and slender clusters with heterogeneous distributions (as shown schematically in Figure S2 of the supporting information).

2.3 Experimental setup used for dropwise condensation

We characterized the wetting stability of the two surfaces under two different situations, 1) for a sessile water droplet, and 2) during dropwise condensation. Here, we define the wetting stability as the capability of a micro/nano structured surface to resist the transition from dewetted Cassie's mode to wetted Wentzel's mode. Figure 2 shows schematically the experimental setup consisting of a thermal control unit, an isolated condensation chamber, and a direct high-speed visualization part, used for the dropwise condensation characterization on these two surfaces. The substrate surface temperature is controlled via a dual stage thermal control unit (1st stage uses a heat sink with a coolant circulator, and 2nd stage uses a Peltier with Labview data acquisition module). The chamber is filled with a mixture of water vapor and nitrogen gas with a preset humidity. A high-speed microphotography is used to capture the condensation process. The sample surfaces are aligned on a cooling stage with constant temperature of 5 ± 0.2^{o}C, where the chamber

ambient temperature and relative humidity are maintained at 25 ± 0.2°C and 40 ± 5%, respectively.

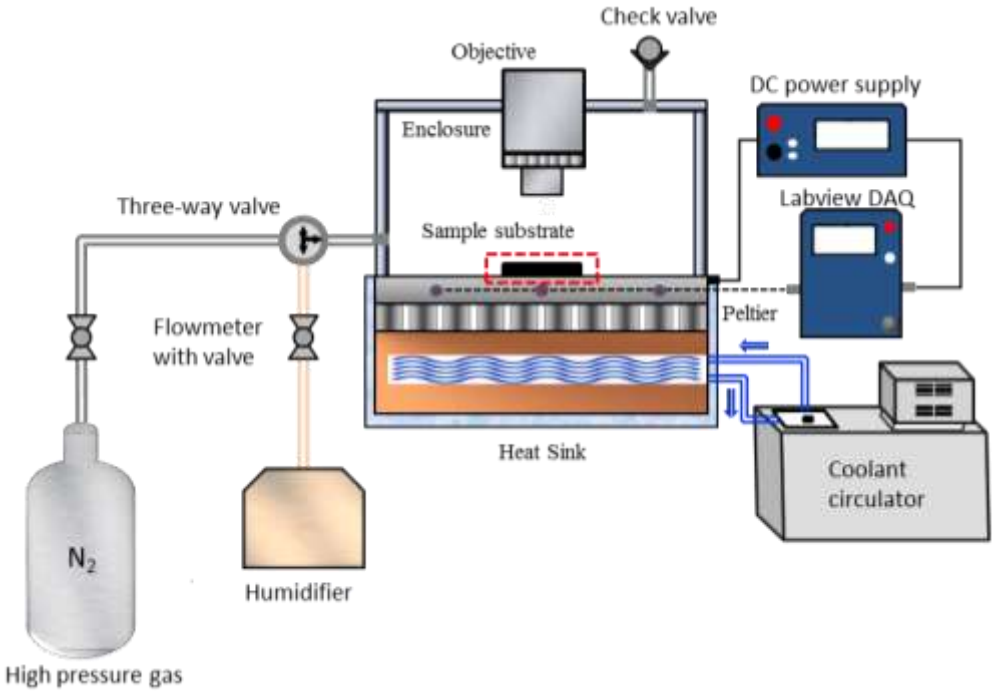

Figure 2. Schematic diagram of the experimental setup used for dropwise condensation tests.

3. Results and discussion

3.1 Wetting stability of a sessile water droplet

3.1.1 Theoretical analysis

When depositing a small water droplet on a rough surface, the combination of surface chemistry and surface asperities (i.e., shape, size and spacing) determines its wetting mode. The wetting transition from Cassie's mode to Wenzel's mode occurs when the surface tension cannot hold against the downward pull of gravity and the liquid penetrates the spaces between asperities, instigating collapse. A mixed coexisting wetting mode has also been reported frequently. The condition to maintain a steady liquid/air interface of a droplet on atop asperities can be analyzed either by the total free energy minimization [42, 43] or the force balancing along the interface

[44, 45]. Extrand's work [44] on this aspect showed clearly that two criteria must be satisfied for a stable Cassie's state, as expressed in equations (1) and (2).

$$\Lambda > \Lambda_c = -\rho g V^{1/3}(1-k)\left\{\tan(\theta_a/2)\left[3+\tan^2(\theta_a/2)\right]\right\}^{2/3} / \left[(36\pi)^{1/3}\gamma\cos\theta_{a,0}\right] \quad (1)$$

$$h > h_c = \Lambda/2\tan\left[\left(\theta_{a,0}-90^o\right)/2\right] \quad (2)$$

Equations (1) and (2) represent the contact line density criterion and the asperity height criterion, respectively. $\Lambda = \pi d/p^2$ is the contact line density, defined as the product of the asperity perimeter and the packing density of asperities $1/p^2$. h is the asperity height, defined as the depth from flat substrate base to the tip of asperities. Λ_c and h_c is the critical contact line density and the critical asperity height, respectively. k is a correction factor, γ is the surface tension of water, ρ is the liquid density, g is gravitational constant, and V is the total volume of a liquid droplet. θ_a and $\theta_{a,0}$ are respectively the apparent advancing angle of the rough surface (e.g., the prepared Surf_1 and Surf_2 in this work) and the true advancing angle for a smooth substrate (as seen in the supporting information of Table S1). Of note the expressions by the two equations were derived without consideration of external disturbances such as phase change [46], hydraulic pressure [42], kinetic impact [47], etc. Direct experimental evidences have shown that a rough surface satisfying the two criteria can still undergo wetting transition from Cassie's mode to Wenzel's mode upon a small external disturbance [48]. It has been established that most surfaces capable of maintaining a stable Cassie's state have densely packed tall and slender asperities (i.e., larger h and p) [49, 50]. We herein introduce a dimensionless parameter $\lambda \equiv \Lambda h/\Lambda_c h_c$ as a stability factor to describe the capability of a surface packed with asperities to resist the wetting transition, with a larger λ indicating a more stable composite Cassie's state.

To allow for quantitatively assessing the wetting behavior of the two sample surfaces with nano-asperities reported in this work, the structure of sample surfaces is modelled as regular arrays with uniformly distributed circular cylinders. Figure 3(a) schematically shows the composite state of a sessile drop on such a structured surface, with *d*, *p* and *h* denoting asperity diameter, pitch (surface to surface) and height, respectively. The mean roughness (defined as the ratio of the true area of the solid surface to the projected surface area) is estimated to be about 2.1 for Surf_1 (d ~ 70 nm, p ~ 120 nm, with the aspect ratio ~ 1) and ~ 1.1 for Surf_2 (d ~ 70 nm, p ~ 300 nm, with the aspect ratio ~ 5). With these parameters, we can obtain that Surf_1 and Surf_2 have the wetting stability factor of λ = 854 and λ = 17.4, respectively. Figure 3(b) shows the variation of wetting stability factor λ with packing density $\psi \equiv \frac{1}{p^2}$. Also, the figure includes several literature results [13, 48, 51] to validate our introduced wetting stability factor λ. Clearly, Figure 3(b) demonstrates that larger λ values always correspond to stable composite Cassie's states, regardless the type of external disturbances due to hydraulic pressure, evaporation, and condensation. Accordingly, it suggests that Surf_1 can maintain a more stable composite Cassie's state which will be shown by our following experimental results.

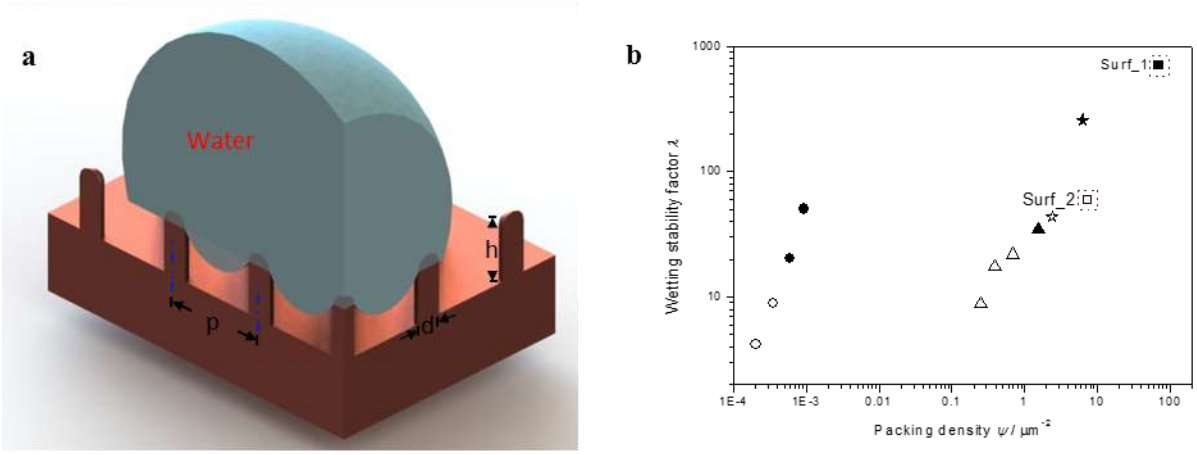

Figure 3. Schematic representation and wetting characterizations of Surf_1 and Surf_2. (a) A schematic illustration showing the state of a sessile droplet on the top of a well-structured surface having nano-asperities, with d, p and h denoting the asperity diameter, pitch and height, respectively. (b) Wetting stability factor λ as a function of packing density of asperities $\psi \equiv \frac{1}{p^2}$ for different types of surfaces. Solid and hollow symbols represent the surface configurations that can sustain a stable or a transit Cassie's mode, respectively. Circles are the results from reference [48], showing the stable and transit Cassie's mode upon increasing the hydraulic pressure. Triangles are the results from reference [51], showing the stable and transit Cassie's mode upon evaporation. Stars are the results from reference [13], showing the stable and transit Cassie's mode upon condensation.

3.1.2 Experimental results

The wetting stability of the prepared Surf_1 and Surf_2 was characterized by measuring the time span of the static contact angle and sliding angle on the two surfaces. A constant volume of 10 μl deionized water drop was gently deposited onto the surfaces through a micropipette. For the case of static contact angle measurements, the sample surfaces were kept horizontally. For the case of sliding angle measurements, the sample surfaces were kept horizontally first, and after a preset time t, the surfaces were gradually inclined until the droplet rolled off.

Figure 4 presents selected time-span images showing the dynamic wetting behaviors of a sessile water drop on Surf_1 and Surf_2 oriented horizontally and with an inclined angle θ_s (under which the drop rolls off after a preset time t = 200 s). Quantitatively, figures 5 (a) and (b) show the measured static contact angle θ and sliding angle θ_s versus time. Figure 5 (c) shows the time variation of wetting fraction f_{SL}, which is computed using the classical Cassie-Baxter equation: $\cos\theta = f_{SL}\cos\theta_0 - 1 + f_{SL}$, where θ_0 = 108.2 ± 3.2° is the static contact angle on the untreated smooth copper surface. When gently deposited, the water drop initially tends to be suspended atop asperities, due to a network of air/water interface connecting individual asperities formed by trapping air pockets underneath the droplet. However, whether the resultant air/water interface

remains stable or is distorted leading to the transition from Cassie's mode to Wenzel's mode under external disturbances is determined by the wetting stability of each individual surface. At the initial stage, the values of the static contact angle θ are 160.2 ± 3.5^o and 158.3 ± 5.7^o for Surf_1 and Surf_2, respectively (see Table S1 in the supporting information). Moreover, the sliding angle θ_s is less than 5^o for both two surfaces, showing that both Surf_1 and Surf_2 are superhydrophobic. As time elapses, no noticeable changes of the static contact angle and the sliding angle on Surf_1 are observed within the observation period of 200 s. The surface could maintain its small sliding angle of $\theta_s < 5^o$ and low wetting fraction f_{SL} of about 0.1 even after 200s. Therefore, one can conclude that Surf_1 is able to maintain its stable Cassie's mode. In contrast, for Surf_2, both its static contact angle and sliding angle are found to drastically vary with time. For instance, within the observation period of 200s, the static contact angle decreases from over 150^o to about 110 ^{o} (close the static contact angle of the untreated smooth copper surface θ_0). Meanwhile, the sliding angle increases from below 5^o to over 60 ^{o}. Furthermore, its wetting fraction f_{SL} increases from slightly below 0.2 to about 0.9. Clearly, there facts suggest that as time elapses, more and more area underneath the water droplet get wetted on Surf_2, and hence Surf_2 undergoes the wetting state transitions from Cassie's mode to Wenzel's mode.

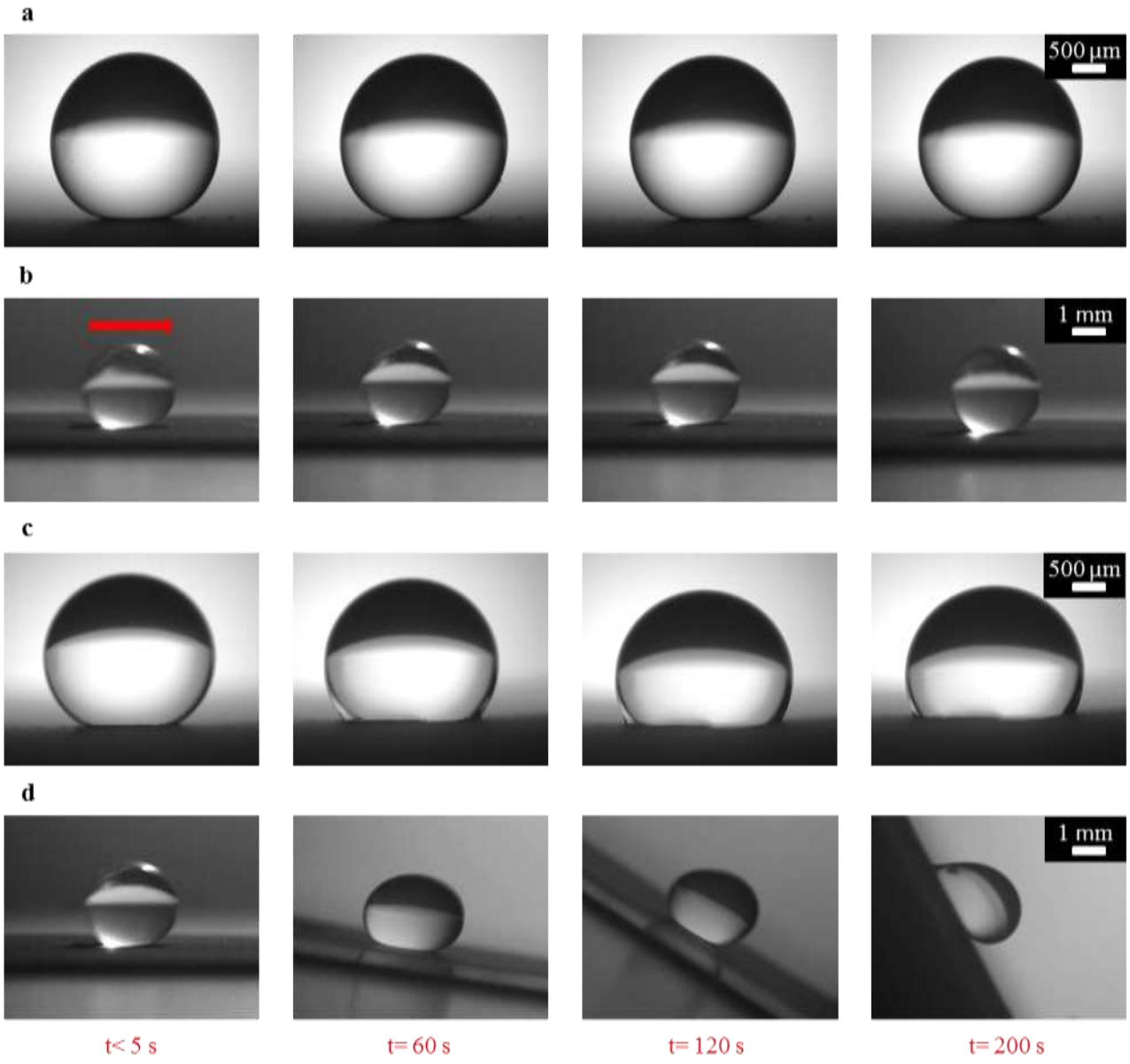

Figure 4. The dynamic wetting behaviors of a 10 µl deionized sessile water drop on Surf_1 and Surf_2. (a) and (b) are the selected time-span images respectively showing the sessile drop on Surf_1 with a horizontal orientation and an inclined angle θ_s (under which the drop rolls off after a preset time t = 200 s). (c) and (d) are the selected time-span images respectively showing the sessile drop on Surf_2 with a horizontal orientation and an inclined angle θ_s (under which the drop rolls off after a preset time t = 200 s).

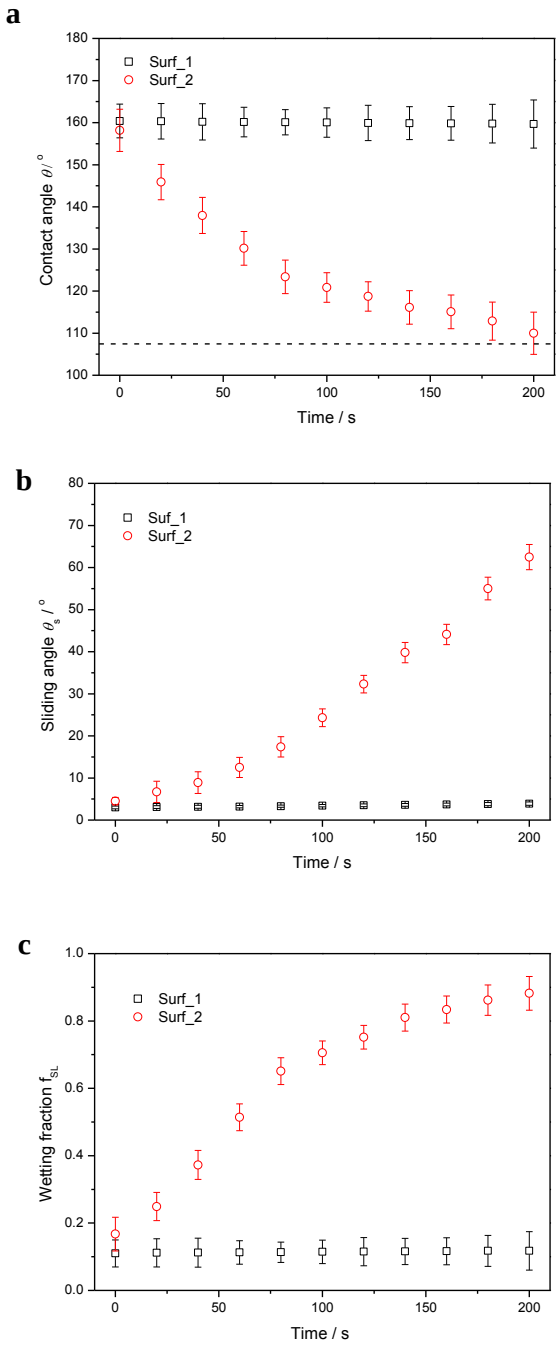

Figure 5. The static contact angle (a), sliding angle (b) and wetting fraction (c) of a gently deposited 10 µl deionized water drop on Surf_1 and Surf_2. Error bars are based on four independent measurements.

3.2 Wetting stability in dropwise condensation

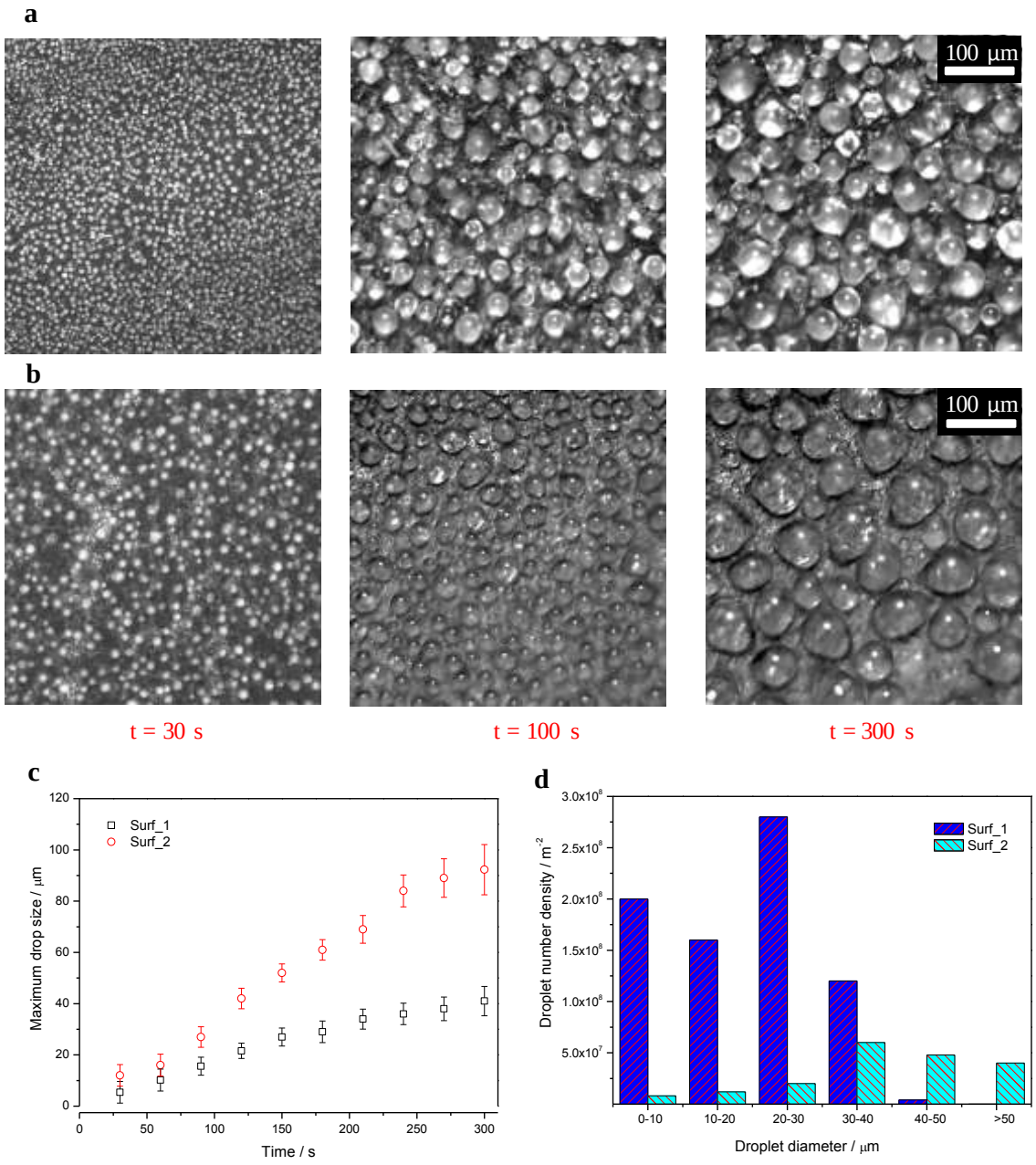

Figure 6. Growth of condensate droplets on horizontal (a) Surf_1 and (b) Surf_2 with a fixed temperature of 5 ± 0.2°C. (c) Maximum size of condensate droplets as a function of time. Error bars are based on four independent measurements. (d) Histograms show the size distributions of condensate droplets.

One of the most important applications of superhydrophobic surfaces is to promote dropwise condensation. Similar to the wetting transition observed using the sessile droplet method [10, 46], wetting transition on rough surfaces with unstable wetting mode also occurs during condensation. The likely mechanism is due to capillary condensation of the liquid water in the surface cavities [52-55].

Figure 6 shows condensation performance of the two surfaces. Initially, more nucleation sites are observed on Surf_1 due to its larger density of asperities. Droplet growth and interdrop coalescences determine the size and distribution of condensate droplets. Both snapshots at 100 s and 300 s show clearly that the characteristic size of the condensate droplets on Surf_2 is much larger than that on Surf_1. The droplet number density, however, is much larger on Surf_1 than that on Surf_2. The wetting state of these condensed droplets can be readily detected through observing the optical reflection of the microsized air pockets underneath the condensate droplets. As expected from our theoretical analysis, the condensate droplets on Surf_1 are in composite Cassie's mode while the condensate droplets on Surf_2 are in Wenzel's mode. Quantitatively, we also characterized the condensation dynamics on the two surfaces by using direct image analysis. Figure 6(c) shows the maximum droplet size as a function of condensation time. The maximum condensate droplet size is around 40 μm on Surf_1 while it approaches to 100 μm on Surf_2. As the maximum droplet size during the condensation process is an important factor that indicates the capability of a surface to maintain long term dropwise condensation, Surf_1 is more suitable for promoting dropwise condensation and thus, enhancing heat transfer. Using the droplet number density in Figure 6(c), we can estimate that the approximate average heat fluxes for Surf_1 and Surf_2 during the observation time are 4.2 ± 0.4 kW/m^2 and 2.7 ± 0.3 kW/m^2, respectively. Figure 6 (d) shows droplet size distribution at the final stage of condensation, i.e.

300 s in the present study. The condensate droplets on Surf_1 vary from less than 10 μm to 30 ~ 40 μm, with no droplets observed beyond 40 μm. In contrast, the condensate droplets on Surf_2 are widely spreaded within a range from 10 μm to over 50 μm.

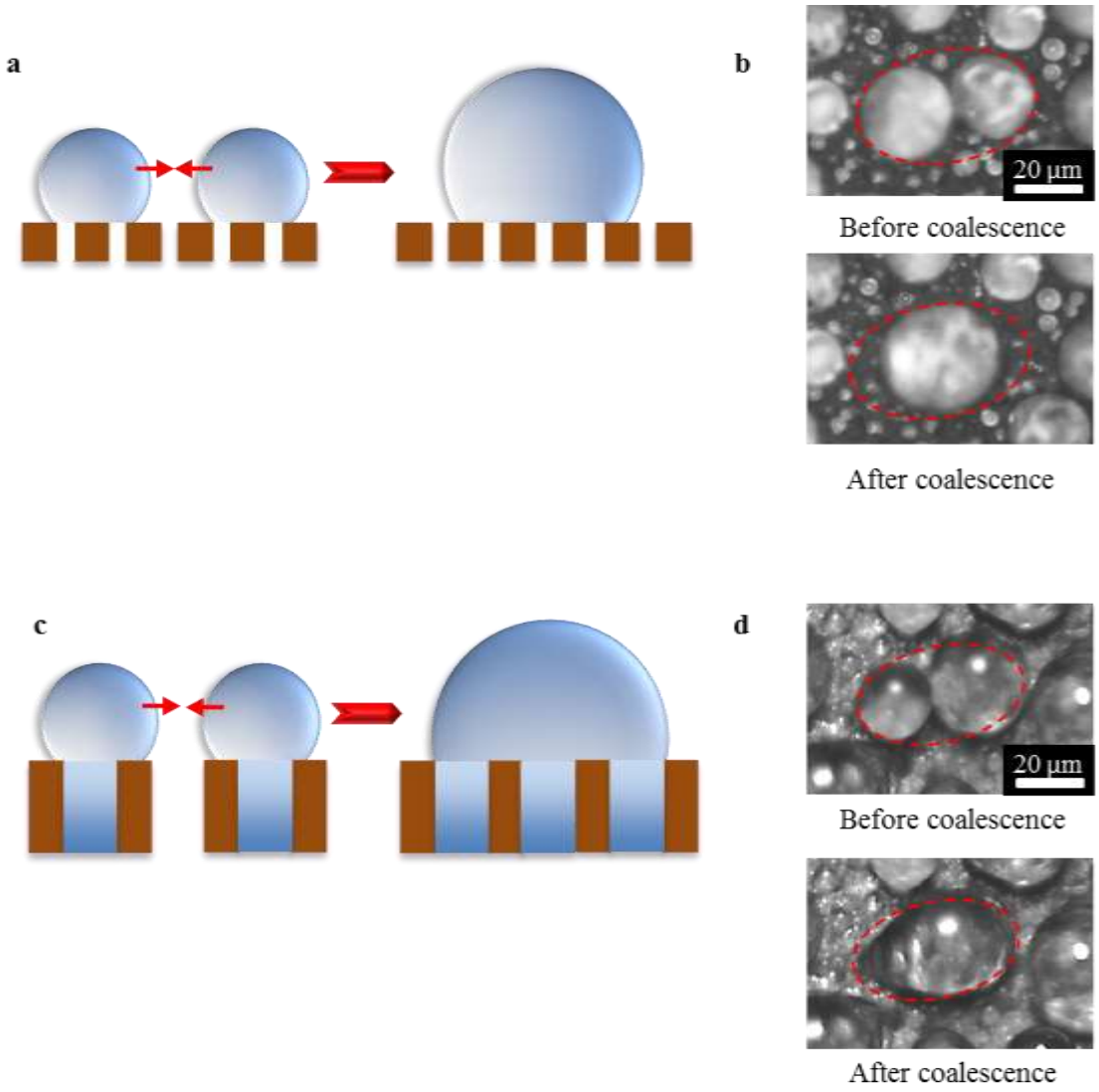

Figure 7. Two regimes of inter-drop coalescence on the surfaces with nano-asperities. (a) and (c) are schematic illustrations of interdrop coalescence between two small drops of Cassie's mode and Wenzel's mode, respectively. (b) and (d) are the corresponding experimental observations of inter-drop coalescence on Surf_1 and Surf_2, respectively.

We attribute the difference in condensation behaviors of these surfaces to two regimes of inter-drop coalescences stemming from the different wetting modes. Figure 7 shows the schematic illustrations and experimental evidence of two coalescence regimes on Surf_1 and Surf_2. For the case of two small droplets in Cassie' mode as on Surf_1, the two droplets merge into one larger droplet with no change in contact angle, while the contact line is de-pined and new contact line is formed. For the case of two small droplets in Wenzel's mode as on Surf_2, the contact line is pined due to the counter-lock of solid/water interfaces, and hence the contact angle changes. As a result, a void is left after an interdrop coalescence on Surf_1. Thus, the sub-sequential interdrop coalescence of the resultant drop is suppressed, preventing its further growth. Differently, the resultant droplet from inter-drop coalescence on Surf_2 has a larger contact line due to decreasing contact angle, without void. Hence, the growth of such a drop is accelerated during further inter-drop coalescence.

Droplet jumping upon coalescence of two adjacent micro drops is another important mechanism that can also reduce the maximum condensate droplet size effectively due to continuous removal of oversized drops. However, droplet jumping requires a much smaller solid fraction of $\phi < 0.1$ as well as, a stable Cassie's mode of wetting [56]. Therefore, this phenomenon was not observed on either of the two surfaces in the present study.

4. Concluding remarks

In this work, we developed two different superhydrophobic surfaces with nanoscale asperities by using a modified electrochemical deposition method. Through varying the deposition rate, the substrate nanostructure and the resultant wetting stability can be altered dramatically as shown in sessile droplet and dropwise condensation cases. For the case of sessile droplets, we investigated

the wetting dynamics of these two surfaces by measuring their static contact angles and sliding angles. The results showed that the wetting transition is strongly related to the geometry and packing density of asperities. We found that the surfaces with coarse nano-asperities of large aspect ratios are not the proper structure to maintain steady superhydrophobic state. In contrast, the surfaces with dense round asperities are more durable superhydrophobic surfaces. The results from the dropwise condensation also showed the same trend.

Our results showed that the modified electrochemical deposition method can allow to effectively and economically fabricate superhydrophobic surfaces of varying scales and complex shapes. We envision that our understanding of the wetting transition and its performance on surfaces with different asperities allows us to construct a wide variety of surfaces out made from routine materials, and such superhydrophobic surfaces can be exploited in condensation and boiling heat transfer, as well as flow control.

ASSOCIATED CONTENT

Supporting Information

The graphical results for the contact angle measurement of smooth surfaces with and without silanization, the table of contact angle measurement results, and the schematic of electrochemical deposition.

AUTHOR INFORMATION

Corresponding Author

*E-mail: mcyang@ntu.edu.sg

Notes

The authors declare no competing financial interest.

ACKNOWLEDGMENTS

We acknowledge the financial support from the Ministry of Singapore via Academic Research Fund (MOE2016-T2-1-114) to CY and YZ and the Nanyang Technological University PhD Scholarship to HZ.

REFERENCES

[1] R. Raj, S. Adera, R. Enright, E.N. Wang, High-resolution liquid patterns via three-dimensional droplet shape control, Nat Commun, 5 (2014).
[2] H.W. Hu, G.H. Tang, D. Niu, Wettability modified nanoporous ceramic membrane for simultaneous residual heat and condensate recovery, Scientific Reports, 6 (2016) 27274.
[3] H. Chen, P. Zhang, L. Zhang, H. Liu, Y. Jiang, D. Zhang, Z. Han, L. Jiang, Continuous directional water transport on the peristome surface of Nepenthes alata, Nature, 532(7597) (2016) 85-89.
[4] Y.G. Zhao, R.Z. Lin, T. Tran, C. Yang, Confined wetting of water on CNT web patterned surfaces, Applied Physics Letters, 111(16) (2017) 161604.
[5] A.R. Betz, D. Attinger, Can segmented flow enhance heat transfer in microchannel heat sinks?, International Journal of Heat and Mass Transfer, 53(19) (2010) 3683-3691.
[6] A.R. Betz, J. Jenkins, C.-J.C. Kim, D. Attinger, Boiling heat transfer on superhydrophilic, superhydrophobic, and superbiphilic surfaces, International Journal of Heat and Mass Transfer, 57(2) (2013) 733-741.
[7] D. Cooke, S.G. Kandlikar, Effect of open microchannel geometry on pool boiling enhancement, International Journal of Heat and Mass Transfer, 55(4) (2012) 1004-1013.
[8] J.S. Mehta, S.G. Kandlikar, Pool boiling heat transfer enhancement over cylindrical tubes with water at atmospheric pressure, Part II: Experimental results and bubble dynamics for circumferential V-groove and axial rectangular open microchannels, International Journal of Heat and Mass Transfer, 64 (2013) 1216-1225.
[9] Y.G. Zhao, C. Yang, Retarded condensate freezing propagation on superhydrophobic surfaces patterned with micropillars, Applied Physics Letters, 108(6) (2016) 061605.
[10] S. Bengaluru Subramanyam, V. Kondrashov, J. Rühe, K.K. Varanasi, Low Ice Adhesion on Nano-Textured Superhydrophobic Surfaces under Supersaturated Conditions, ACS Applied Materials & Interfaces, 8(20) (2016) 12583-12587.
[11] S. Wiedemann, A. Plettl, P. Walther, P. Ziemann, Freeze Fracture Approach to Directly Visualize Wetting Transitions on Nanopatterned Superhydrophobic Silicon Surfaces: More than a Proof of Principle, Langmuir, 29(3) (2012) 913-919.
[12] N. Miljkovic, D.J. Preston, R. Enright, E.N. Wang, Electrostatic charging of jumping droplets, Nat Commun, 4 (2013).
[13] N. Miljkovic, E.N. Wang, Condensation heat transfer on superhydrophobic surfaces, MRS Bulletin, 38(05) (2013) 397-406.

[14] Y. Zhao, R. Wang, C. Yang, Interdroplet freezing wave propagation of condensation frosting on micropillar patterned superhydrophobic surfaces of varying pitches, International Journal of Heat and Mass Transfer, 108, Part A (2017) 1048-1056.
[15] T.M. Schutzius, S. Jung, T. Maitra, G. Graeber, M. Köhme, D. Poulikakos, Spontaneous droplet trampolining on rigid superhydrophobic surfaces, Nature, 527(7576) (2015) 82-85.
[16] N. Miljkovic, R. Enright, Y. Nam, K. Lopez, N. Dou, J. Sack, E.N. Wang, Jumping-Droplet-Enhanced Condensation on Scalable Superhydrophobic Nanostructured Surfaces, Nano Letters, (2012).
[17] M. He, Q. Zhang, X. Zeng, D. Cui, J. Chen, H. Li, J. Wang, Y. Song, Hierarchical Porous Surface for Efficiently Controlling Microdroplets' Self-Removal, Advanced Materials, 25(16) (2013) 2291-2295.
[18] C.-H. Xue, X.-J. Guo, J.-Z. Ma, S.-T. Jia, Fabrication of Robust and Antifouling Superhydrophobic Surfaces via Surface-Initiated Atom Transfer Radical Polymerization, ACS Applied Materials & Interfaces, 7(15) (2015) 8251-8259.
[19] P. Papadopoulos, D. Vollmer, H.-J. Butt, Long-Term Repellency of Liquids by Superoleophobic Surfaces, Physical Review Letters, 117(4) (2016) 046102.
[20] Y. Zhao, C. Zhao, J. He, Y. Zhou, C. Yang, Collective effects on thermophoresis of colloids: a microfluidic study within the framework of DLVO theory, Soft Matter, 9(32) (2013) 7726-7734.
[21] Y. Huang, H. Li, T.N. Wong, Two immiscible layers of electro-osmotic driven flow with a layer of conducting non-Newtonian fluid, International Journal of Heat and Mass Transfer, 74 (2014) 368-375.
[22] D. Das, D.-T. Phan, Y. Zhao, Y. Kang, V. Chan, C. Yang, A multi-module microfluidic platform for continuous pre-concentration of water-soluble ions and separation of oil droplets from oil-in-water (O/W) emulsions using a DC-biased AC electrokinetic technique, ELECTROPHORESIS, 38(5) (2017) 645-652.
[23] Y. Huang, L. Xiao, T. An, W. Lim, T. Wong, H. Sun, Fast Dynamic Visualizations in Microfluidics Enabled by Fluorescent Carbon Nanodots, Small, 13(34) (2017) 1700869-n/a.
[24] V. Hejazi, M. Nosonovsky, Wetting Transitions in Two-, Three-, and Four-Phase Systems, Langmuir, 28(4) (2011) 2173-2180.
[25] V. Hejazi, A.E. Nyong, P.K. Rohatgi, M. Nosonovsky, Wetting Transitions in Underwater Oleophobic Surface of Brass, Advanced Materials, 24(44) (2012) 5963-5966.
[26] D. Murakami, H. Jinnai, A. Takahara, Wetting Transition from the Cassie–Baxter State to the Wenzel State on Textured Polymer Surfaces, Langmuir, 30(8) (2014) 2061-2067.
[27] Z. Yilei, S. Sriram, Superhydrophobic engineering surfaces with tunable air-trapping ability, Journal of Micromechanics and Microengineering, 18(3) (2008) 035024.
[28] K. Rykaczewski, A.T. Paxson, S. Anand, X. Chen, Z. Wang, K.K. Varanasi, Multimode Multidrop Serial Coalescence Effects during Condensation on Hierarchical Superhydrophobic Surfaces, Langmuir, 29(3) (2012) 881-891.
[29] Y. Zhao, C. Yang, Frost spreading on microscale wettability/morphology patterned surfaces, Applied Thermal Engineering, 121 (2017) 136-145.
[30] H. Zhang, Y. Zhao, R. Lv, C. Yang, Freezing of sessile water droplet for various contact angles, International Journal of Thermal Sciences, 101 (2016) 59-67.
[31] M. Kahani, R.G. Jackson, G. Rosengarten, Experimental Investigation of TiO2/Water Nanofluid Droplet Impingement on Nanostructured Surfaces, Industrial & Engineering Chemistry Research, 55(7) (2016) 2230-2241.
[32] A. Marmur, Wetting on Hydrophobic Rough Surfaces: To Be Heterogeneous or Not To Be?, Langmuir, 19(20) (2003) 8343-8348.
[33] R. Wen, Z. Lan, B. Peng, W. Xu, R. Yang, X. Ma, Wetting Transition of Condensed Droplets on Nanostructured Superhydrophobic Surfaces: Coordination of Surface Properties and Condensing Conditions, ACS Applied Materials & Interfaces, 9(15) (2017) 13770-13777.

[34] C. Lv, P. Hao, X. Zhang, F. He, Dewetting Transitions of Dropwise Condensation on Nanotexture-Enhanced Superhydrophobic Surfaces, ACS Nano, 9(12) (2015) 12311-12319.
[35] W. Ren, Wetting Transition on Patterned Surfaces: Transition States and Energy Barriers, Langmuir, 30(10) (2014) 2879-2885.
[36] D.-H. Jung, A. Sharma, K.-H. Kim, Y.-C. Choo, J.-P. Jung, Effect of Current Density and Plating Time on Cu Electroplating in TSV and Low Alpha Solder Bumping, Journal of Materials Engineering and Performance, 24(3) (2015) 1107-1115.
[37] D. Grujicic, B. Pesic, Electrodeposition of copper: the nucleation mechanisms, Electrochimica Acta, 47(18) (2002) 2901-2912.
[38] D. Grujicic, B. Pesic, Reaction and nucleation mechanisms of copper electrodeposition from ammoniacal solutions on vitreous carbon, Electrochimica Acta, 50(22) (2005) 4426-4443.
[39] B.-K. Pong, H.I. Elim, J.-X. Chong, W. Ji, B.L. Trout, J.-Y. Lee, New Insights on the Nanoparticle Growth Mechanism in the Citrate Reduction of Gold(III) Salt: Formation of the Au Nanowire Intermediate and Its Nonlinear Optical Properties, The Journal of Physical Chemistry C, 111(17) (2007) 6281-6287.
[40] J.B. Boreyko, Y. Zhao, C.-H. Chen, Planar jumping-drop thermal diodes, Applied Physics Letters, 99(23) (2011) 234105.
[41] M.E. Hyde, R.G. Compton, A review of the analysis of multiple nucleation with diffusion controlled growth, Journal of Electroanalytical Chemistry, 549 (2003) 1-12.
[42] Q.S. Zheng, Y. Yu, Z.H. Zhao, Effects of Hydraulic Pressure on the Stability and Transition of Wetting Modes of Superhydrophobic Surfaces, Langmuir, 21(26) (2005) 12207-12212.
[43] E. Bormashenko, Wetting transitions on biomimetic surfaces, Philosophical Transactions of the Royal Society A: Mathematical, Physical and Engineering Sciences, 368(1929) (2010) 4695-4711.
[44] C.W. Extrand, Criteria for Ultralyophobic Surfaces, Langmuir, 20(12) (2004) 5013-5018.
[45] C.-H. Choi, C.-J.C. Kim, Droplet Evaporation of Pure Water and Protein Solution on Nanostructured Superhydrophobic Surfaces of Varying Heights, Langmuir, 25(13) (2009) 7561-7567.
[46] C.E. Clavijo, J. Crockett, D. Maynes, Wenzel to Cassie transition during droplet impingement on a superhydrophobic surface, Physical Review Fluids, 1(7) (2016) 073902.
[47] H. Kim, C. Lee, M.H. Kim, J. Kim, Drop Impact Characteristics and Structure Effects of Hydrophobic Surfaces with Micro- and/or Nanoscaled Structures, Langmuir, 28(30) (2012) 11250-11257.
[48] B. He, N.A. Patankar, J. Lee, Multiple Equilibrium Droplet Shapes and Design Criterion for Rough Hydrophobic Surfaces, Langmuir, 19(12) (2003) 4999-5003.
[49] Y. Hou, M. Yu, X. Chen, Z. Wang, S. Yao, Recurrent Filmwise and Dropwise Condensation on a Beetle Mimetic Surface, ACS Nano, 9(1) (2015) 71-81.
[50] G.S. Watson, B.W. Cribb, J.A. Watson, How Micro/Nanoarchitecture Facilitates Anti-Wetting: An Elegant Hierarchical Design on the Termite Wing, ACS Nano, 4(1) (2010) 129-136.
[51] A. Bussonniere, M.B. Bigdeli, D.-Y. Chueh, Q. Liu, P. Chen, P.A. Tsai, Universal wetting transition of an evaporating water droplet on hydrophobic micro- and nano-structures, Soft Matter, 13(5) (2017) 978-984.
[52] A.J. Meuler, G.H. McKinley, R.E. Cohen, Exploiting Topographical Texture To Impart Icephobicity, ACS Nano, 4(12) (2010) 7048-7052.
[53] K.K. Varanasi, M. Hsu, N. Bhate, W. Yang, T. Deng, Spatial control in the heterogeneous nucleation of water, Applied Physics Letters, 95(9) (2009) 094101.
[54] H.W. Hu, G.H. Tang, D. Niu, Experimental investigation of condensation heat transfer on hybrid wettability finned tube with large amount of noncondensable gas, International Journal of Heat and Mass Transfer, 85 (2015) 513-523.
[55] R. Wen, Q. Li, J. Wu, G. Wu, W. Wang, Y. Chen, X. Ma, D. Zhao, R. Yang, Hydrophobic copper nanowires for enhancing condensation heat transfer, Nano Energy, 33 (2017) 177-183.

[56] J.B. Boreyko, C.P. Collier, Delayed Frost Growth on Jumping-Drop Superhydrophobic Surfaces, ACS Nano, 7(2) (2013) 1618-1627.